

## Article

# Nanocellulose Extracted from Paraguayan Residual Agro-Industrial Biomass: Extraction Process, Physicochemical and Morphological Characterization

Maria Edelira Velázquez<sup>1</sup>, Omayra Beatriz Ferreiro<sup>1,2</sup>, Diego Batista Menezes<sup>3</sup>, Yendry Corrales-Ureña<sup>3,4</sup> , José Roberto Vega-Baudrit<sup>3,5</sup>  and Juan Daniel Rivaldi<sup>2,\*</sup> 

<sup>1</sup> Facultad de Comunicación, Arte y Ciencias de la Tecnología, Universidad Americana, Asunción 1206, Paraguay

<sup>2</sup> Facultad de Ciencias Químicas, Universidad Nacional de Asunción, San Lorenzo 111421, Paraguay

<sup>3</sup> Laboratorio Nacional de Nanotecnología LANOTEC, CENAT, Pavas, San José 10109, Costa Rica

<sup>4</sup> Faculty of Production Engineering, University of Bremen, Am Fallturm 1, 28359 Bremen, Germany

<sup>5</sup> Laboratorio de Polímeros, Escuela de Química, Universidad Nacional, Heredia 40104, Costa Rica

\* Correspondence: danielrivaldi@gmail.com

**Abstract:** Residual biomasses from agro-industries in Paraguay, including soybean hulls (SBHs) and sugarcane bagasse (SCB), were studied as a source for nanocellulose extraction for the first time. For that purpose, both biomasses were delignified in a semi-pilot stainless-steel reactor, and the cellulose pulp was subjected to a bleaching process with NaClO (2.5%, *w/v*). The nanocellulose (CNC) was obtained after two-step acid hydrolysis. Firstly, the bleached cellulose was hydrolyzed with HCl (17%, *w/w*) for two hours at 60 °C to obtain microcrystals by removing most of the amorphous fraction. The celluloses were then treated with H<sub>2</sub>SO<sub>4</sub> (65%, *w/w*) at 45 °C for 45 min to obtain nanocellulose. Physicochemical and morphological properties were analyzed using attenuated total reflectance Fourier transform infrared spectroscopy (ATR-FTIR), thermogravimetric analysis (TGA), scanning electron microscopy (SEM), atomic force microscopy (AFM), and X-ray diffraction analysis (XRD). The SBHs nanocellulose had a whisker-like form with a 230 ± 42 nm diameter and a 12 ± 2 nm height, and the SCB nanocellulose had a fibril-like form with a 103 ± 30 nm diameter and a height of 6 ± 3 nm. The nanocellulose from SBHs and SCB had good thermal stability as its degradation temperature started at 250 °C. Furthermore, the nanocellulose obtained was negatively charged and formed stable dispersion in water at 0.1 mg/mL concentration and a pH of around 6.5.

**Keywords:** residual biomass; soybean hulls; sugarcane bagasse; acid hydrolysis; nanocellulose



check for updates

**Citation:** Velázquez, M.E.; Ferreiro, O.B.; Menezes, D.B.; Corrales-Ureña, Y.; Vega-Baudrit, J.R.; Rivaldi, J.D. Nanocellulose Extracted from Paraguayan Residual Agro-Industrial Biomass: Extraction Process, Physicochemical and Morphological Characterization. *Sustainability* **2022**, *14*, 11386. <https://doi.org/10.3390/su141811386>

Academic Editors: María Cristina Area and María Evangelina Vallejos

Received: 7 July 2022

Accepted: 21 August 2022

Published: 10 September 2022

**Publisher's Note:** MDPI stays neutral with regard to jurisdictional claims in published maps and institutional affiliations.



**Copyright:** © 2022 by the authors. Licensee MDPI, Basel, Switzerland. This article is an open access article distributed under the terms and conditions of the Creative Commons Attribution (CC BY) license (<https://creativecommons.org/licenses/by/4.0/>).

## 1. Introduction

The Paraguayan economy is highly dependent on the agricultural and forestry export sector [1]. The processing of agricultural raw materials leads to the generation of large volumes of residual biomass, including sugarcane bagasse, soybean hulls, rice husks, and corn residues [2]. These residues are generally used for animal feed or cover soils, providing organic matter and protection against erosion.

The current major challenge in the world is to develop technologies that allow the valorization of such residues to increase production efficiency by obtaining high-value-added products, such as micro- and nanocellulose [3]. The SBH and SCB biomasses contain cellulose, hemicellulose, and lignin. Cellulose is a linear polysaccharide with more than 4000 monomeric glucose units linked by β-1,4-glycosidic bonds, representing between 30 and 50% of the biomass composition, with highly crystalline structural fractions and amorphous fractions [4–7].

The interest in the extraction and use of micro- and nanocellulose from waste biomass has shown remarkable growth in recent years due to the renewable nature, availability,

and, mainly, the physicochemical and mechanical properties of this type of material [8–10]. CNC consists of rod-shaped cellulose crystals or fibrils, with widths and lengths of 5–70 nm and between 100 nm and several micrometers, respectively [11–13].

Nanocellulose extraction requires the treatment of the biomass by chemical and/or physical methods, such as ultrasonic technique, microwave radiation, enzymatic hydrolysis, and alkaline and acid hydrolysis [14,15], to obtain pure cellulose, followed by the transformation to cellulose nanocrystals [16]. Usually, alkaline hydrolysis followed by acid hydrolysis of residual biomass using sulfuric acid and or hydrochloric acid allows rapid removal of amorphous cellulose to obtain highly crystalline nanofibers [5]. The utilization of sulfuric acid allows the stabilizing of the colloidal system formed by the CNC due to the esterification of the hydroxyl groups by sulfate ions, giving rise to a sulfate group ( $-O-SO_3^-$ ) on the surface. When hydrochloric acid is used instead of sulfuric acid, the tendency is to form aggregates of CNC [17–20]. Wang et al [20] demonstrated that the combination of sulfuric and hydrochloric acids allows better thermal stability of the nanocellulose than when using pure sulfuric acid.

Besides the traditional inorganic acids cited, nitric acid, phosphoric acid, oxalic acid, maleic acid, citric acid, *p*-toluenesulfonic acid, and mixtures of organic and inorganic acids have also been used for micro- and nanocellulose extraction [21–25]. The size of nanocellulose fibers or CNCs varies depending on the acid concentration, hydrolysis temperature, crystallinity degree, and the starting cellulose polymerization degree [4,10,26,27].

Nanocellulose exhibits high stiffness and mechanical strength, with elastic modulus between 150 and 250 GPa, flexural strength in the range of 13–24 GPa, high specific surface area, and properties that enable its use for reinforcing and increasing the strength of other materials [13]. This material finds essential applications in the food industry as an emulsion stabilizer and thickener, reinforcing filler for polymers used for packaging, and as an excipient in the pharmaceutical and cosmetic industries [10,28].

The availability of soybean hulls and sugarcane bagasse residues in Paraguay makes this country a potential nanocellulose supplier. These residual biomasses are characterized by a high cellulose content relative to the lignin content (less than 22% *w/w*), in addition to their abundance and spatial distribution in the Paraguayan territory (Figure 1). These considerations highlight the potential of these residues for obtaining micro- and nanocellulose. In this respect, considering the residue per product rate (RPR), corresponding to 0.06 t soybean hulls/t soybean and 0.290 t bagasse/t sugarcane, and the average annual processing volume of these agriculture feedstocks for the period 2015–2020, an average amount of sugarcane bagasse and soybean hulls in Paraguay of 1,950,000 t/year and 211,000 t/year, respectively, was estimated [2,29].

In the first instance, it could indicate that cost is the limiting factor for obtaining cellulose and micro- and nanocellulose from these biomasses. In Paraguay, the cost of soybean hulls exceeds USD 120/t, while sugarcane bagasse costs USD 24/t [30,31]. However, the estimated annual volume of cellulose nanomaterials required (for manufacturing packaging, paper coating, and fabrics) is about 33 million metric tons for the global market. Its market is expected to grow from USD 346 million in 2021 to USD 963 million by 2026 [32]. The estimated prices for cellulose nanomaterials range from USD 1100/ton to USD 4400/ton [9]. This way, the added value that could be given to both residual biomasses could reach around 40 times if we assume that the residue values are those mentioned above.

This work describes nanocellulose extraction from SBH and SCB using bleaching, alkaline, and acid hydrolysis processes in Paraguay for the first time. Characterization techniques such as scanning electron microscopy (SEM), atomic force microscopy (AFM), attenuated total reflectance Fourier transform infrared spectroscopy (ATR-FTIR), X-ray diffraction analysis (XRD), thermogravimetric analysis (TGA), differential scanning calorimetry (DSC), and zeta potential analysis were used to analyze the extracted materials.

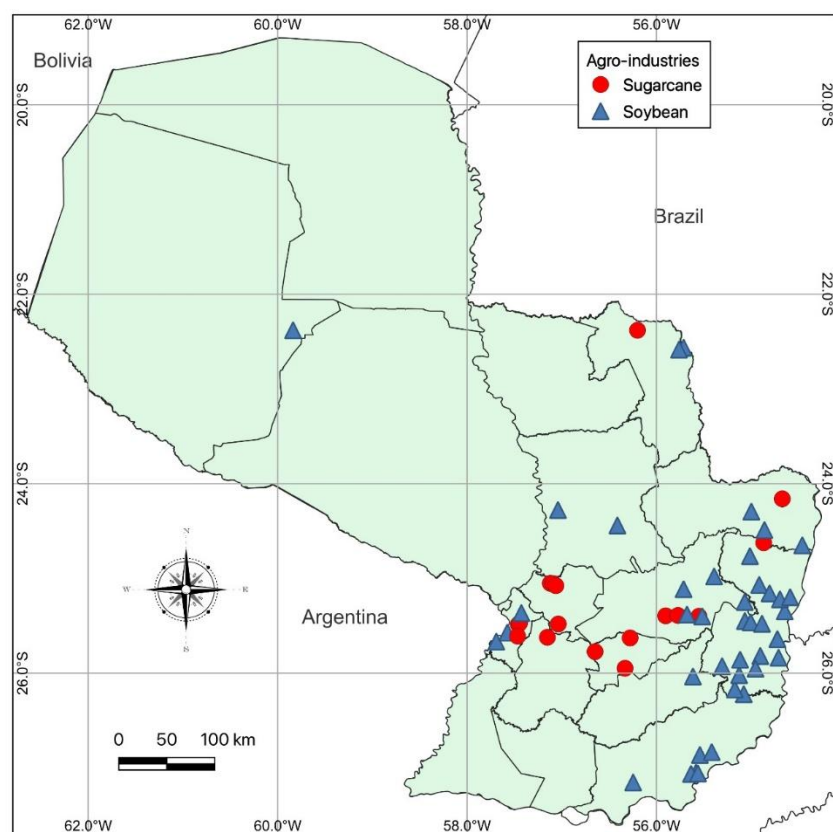


**Figure 1.** Geographical distribution of soybean and sugarcane processing industries in Paraguay.

## 2. Material and Methods

### 2.1. Materials

Soybean hulls (Figure 2a) were provided by Cargill S.A (Minga Guazú, Paraguay), and sugarcane bagasse (Figure 2b) was obtained from Destilería Luis Mussi (Piribebuy, Paraguay). The residual biomasses were dried at 105 °C for 24 h, finely ground in a hammer mill, and sieved with 400 and 300 µm mesh sieves. The cellulose, hemicellulose, and lignin content of the finely separated material was characterized.

### 2.2. Residual Biomass Characterization

Crude fiber, neutral detergent fiber (NDF), acid detergent fiber (ADF), and acid detergent lignin (ADL) were determined in an automated fiber analyzer, Fibretherm FT 12 (C. Gerhardt GmbH & Co. KG Königswinter, Germany), using the FibreBag method. The analysis complies with the standard methods specified by Weender and van Soest. The samples were digested with H<sub>2</sub>SO<sub>4</sub> and NaOH in a filter bag for the fiber content determination. Cellulose and hemicellulose content was calculated by subtracting the ADL and ADF value, respectively, from NDF. Crude ash content was determined according to the standard method ISO 5984:2002.

### 2.3. Alkaline Hydrolysis

The raw materials were subjected to alkaline hydrolysis in a 10 L stainless-steel reactor (Ingest S.A, Buenos Aires, Argentina) in a 2-stage process to remove lignin, according to Camacho et al. [27]. In both stages, the ratio of solid to liquid used was 1:10. In the first stage, hydrolysis was carried out using NaOH (20%, w/v) for 1.5 h at 70 °C and washing with distilled water. Then, the material was hydrolyzed again to increase the lignin removal using NaOH (12%, w/v) for 1.0 h at the same temperature. The material was filtered on polypropylene mesh and washed with deionized water to neutral pH. The resulting cellulose was kept wet for the bleaching process.



**Figure 2.** Soybean hulls (a) and sugarcane bagasse (b) used as feedstock for nanocellulose extraction.

#### 2.4. Bleaching Process

The delignified cellulose was subjected to a bleaching process with NaClO (2.5%, *w/v*) at 60 °C for 2 h. The bleached cellulose pulp was separated by filtration and washed with deionized water several times to remove the bleaching agent.

#### 2.5. Nanocellulose Preparation

The applied protocol was based on the process reported by Camacho et al. [27] for nanocellulose extraction from pineapple residues. The bleached cellulose was subjected to acid hydrolysis in two stages. Firstly, a partial hydrolysis was performed using an HCl solution (17% *w/w*) for 2 h at 60 °C to obtain microcellulose, followed by hydrolysis with H<sub>2</sub>SO<sub>4</sub> (65% *w/w*) at 45 °C under constant stirring for 45 min to prepare nanocrystalline cellulose. This step was carried out on a smaller scale. At the end of the process, the solid material was filtered and washed with deionized water repeatedly until neutral pH was achieved. The suspension containing nanocellulose was sonicated in an ultrasonic bath for 15 min in order to form a stable suspension and then dialyzed on a regenerated cellulose membrane for 24 h to remove excess acid. Finally, the samples were frozen and lyophilized for preservation [27].

#### 2.6. Physicochemical and Structural Characterization of Materials

##### 2.6.1. ATR-FTIR Analysis

The previously pulverized and dried samples were analyzed, and the spectra were recorded on a Thermo Scientific™ Nicolet 6700 spectrometer (Thermo Scientific, Waltham, MA, USA), with a spectral resolution of 4 cm<sup>-1</sup> and a spectral range of 500–4000 cm<sup>-1</sup>. The results were analyzed with OMNIC 8.1 software (OMNIC Series 8.1.10, Thermo Fischer Scientific, Waltham, MA, USA) [27].

##### 2.6.2. Superficial Morphology

The material morphology was analyzed using a scanning electron microscope (SEM), JEOL JSM-6390LV (Jeol USA Inc., Peabody, MA, USA), at an accelerating voltage of 10 kV with secondary electrons (SEI) and a spot size of 40. The hydrolyzed and raw samples were previously coated with a 10 µm gold film.

### 2.6.3. Topographic Analysis

The topography of the nanocellulose samples was analyzed using an atomic force microscope (AFM), Asylum Research (Oxford Instruments, Santa Barbara, CA, USA), operated in air tapping mode. The silicon AFM (Tap150AL-G) probe with the back side of the cantilever covered with Al (Aluminum) was operated at a resonant frequency of 150 kHz and a constant force of 5 N/m.

### 2.6.4. Thermogravimetric Analysis

Thermogravimetric analysis (TGA) was performed using a TGA-Q500 thermogravimetric analyzer (TA Instruments, New Castle, DE, USA), equipped with Universal Analysis 2000 software version 4.5A (TA Instruments, New Castle, DE, USA). Samples of approximately 5.8 mg were placed in a pre-weighed standard platinum tray, and the analysis was conducted with a nitrogen purge flow rate of 10 mL/min for the balance and a purge flow rate of 90 mL/min for the sample. Initially, the equipment was kept at equilibrium at 25 °C for 1 min. Subsequently, heating was performed at 10 °C/min, and changes in mass were recorded in a temperature range from 25 to 1000 °C.

### 2.6.5. Crystallinity Analysis

Samples were analyzed using an X'Pert3 Powder Diffractometer (Malvern Panalytical, Malvern, UK) using a nickel-filtered CuK $\alpha$  radiation at 45 kV and 40 mA, 2 $\theta$  in the range of 10–40° with 0.03° and 1.5 s spacing. The degree of crystallinity was calculated using the following equation (Equation (1)):

$$\% \text{ Crystallinity} = (1 - I_{\text{am}}/I_{002}) \times 100 \quad (1)$$

where

$I_{002}$  = is the maximum intensity at  $2\theta = 22.3^\circ$ ;

$I_{\text{am}}$  = corresponds to the intensity of the minimum.

### 2.6.6. Differential Calorimetric Analysis

The thermal behavior of the samples was studied in a DSC Q200 differential scanning calorimeter (TA Instruments, New Castle, DE, USA). The approximately 2.3 mg sample was heated from 20 to 150 °C at a heating rate of 5 °C/min. Thermograms were used to determine thermal events related to initial melting and crystallization temperatures.

### 2.6.7. Zeta Potential Measurements

Zeta potential ( $\zeta$ ) of aliquots of the aqueous suspension of CNC was measured using a Zetasizer Nano S90 (Malvern Panalytical, Malvern, UK) at  $\lambda_1 = 628$  nm and  $\lambda_2 = 523$  nm, without adjusting ionic strength. The  $\zeta$ -potential was determined by electrophoretic mobility of the particles of SBH and SCB in solution (0.1 mg/mL) at a pH of 6.83 and 6.58, respectively. Five measurements were conducted for each suspension, and the mean and standard deviation were reported.

### 2.7. Nanocellulose Extraction Efficiency

The efficiency of micro- and nanocellulose extraction from soybean hulls and sugarcane bagasse was calculated according to Equation (2):

$$\text{Extraction efficiency } \eta = P_1/P_0 \times X_0 \quad (2)$$

where:

$P_0$  = mass of feedstock submitted to hydrolysis, g;

$P_1$  = mass of micro- and nanocellulose from the acid hydrolysis, g;

$X_0$  = cellulose mass fraction in the feedstock.

### 3. Results and Discussion

Table 1 shows the soybean hull and sugarcane bagasse raw material composition. As can be seen, both residues exhibit a high content of cellulose relative to the lignin content. This allows the use of a less aggressive process to carry out cellulose extraction.

**Table 1.** Composition of agro-industrial residual biomass for nanocellulose extraction.

Parameter	Soybean Hull	Sugarcane Bagasse	Method
Crude fiber, %	41.32	47.48	FibreBag
Neutral detergent fiber, %	62.38	76.66	FibreBag
Acid detergent fiber, %	49.79	58.79	FibreBag
Acid detergent lignin, %	2.66	14.64	FibreBag
Cellulose, %	47.13	44.5	Calculated
Hemicellulose, %	12.59	17.87	Calculated
Ash, %	4.30	8.45	ISO 5984:2002

Figure 3 shows the ATR-FTIR spectra of sugarcane and soybean bagasse raw material and of samples after alkaline hydrolysis. Although peaks from the hemicellulose and lignin overlap with the ones from the cellulose, the spectra of the biomass subjected to chemical treatment presented peaks characteristic of cellulose. Samples of biomasses subjected to alkaline treatment were analyzed for the presence of aryl groups, characteristic of lignin. Structurally, lignin is a three-dimensional macromolecule of aromatic nature composed of aryl ethers connected by various bonds that form a complex and amorphous branched structure [33]. The peak related to the vibration of distinct C-O aryl groups is observed in the range of 1250–1255  $\text{cm}^{-1}$  (Figure 3a–c), present in both sugarcane bagasse and raw soybean hulls [4,34]. However, this peak is not observed in samples chemically treated.

The peak at 1730  $\text{cm}^{-1}$  in the FTIR spectra of raw SCB and raw SBHs is predominantly attributed to the C=O vibration of the acetyl and uronic ester groups of hemicellulose or the ester bond of the carboxylic group of ferulic and *p*-coumaric acids of lignin [8,35]. For the alkaline-treated samples, no comparable peaks were observed in the spectra of treated biomass, indicating that most of the hemicellulose and lignin was removed.

For the raw soybean hulls, the peaks around 1300–1400  $\text{cm}^{-1}$  could be attributed to the presence of hemicellulose and lignin, which are not presented in the spectra of the sample treated by alkaline hydrolysis [36].

The raw materials and alkaline chemically treated spectra present a broad band in the region of 3600–3100  $\text{cm}^{-1}$ , characteristic of a stretching vibration of O-H groups in cellulose molecules [26]. Moreover, the spectra showed peaks corresponding to the vibration of C-H bonds close to 2890  $\text{cm}^{-1}$  and those corresponding to C-H and C-O bonds of polysaccharide rings at 1330–1360  $\text{cm}^{-1}$  [27]. The peak at 1060  $\text{cm}^{-1}$  in all samples is associated with cellulose, which has a higher intensity in the alkaline-treated samples [37].

The peak near 2900  $\text{cm}^{-1}$  has a higher intensity in the sugarcane bagasse sample after the hydrolysis. This could be attributed to removing the non-cellulosic material without affecting the cellulose [27,37]. The peak near 1640  $\text{cm}^{-1}$  present in all spectra is attributed to the absorption of water that is bonded to the cellulose, and it is higher in samples with higher cellulose content [11,36,37].

In this sense, the SBH spectra showed that the alkaline hydrolysis affected the cellulose structure as can be seen from the changes observed in the peaks at 2900  $\text{cm}^{-1}$  and 1640  $\text{cm}^{-1}$ . In the nanocellulose spectra of sugarcane bagasse and soybean hulls, a band at 900–910  $\text{cm}^{-1}$  is distinguishable and associated with  $\beta$ -glycosidic bonds of crystalline cellulose molecules [8,38].

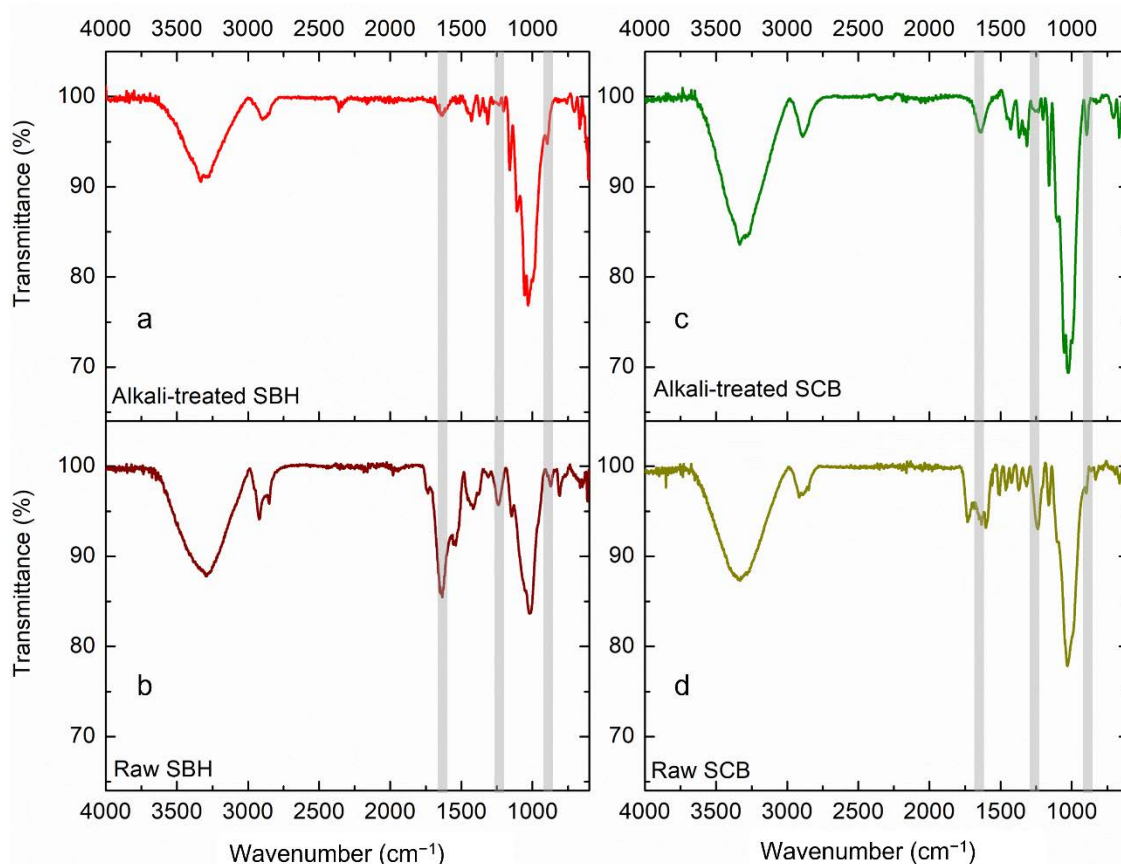


**Figure 3.** ATR-FTIR spectroscopy of alkali-treated soybean hulls (a), raw soybean hulls (b), alkali-treated sugarcane bagasse (c), and raw sugarcane bagasse (d) for wavelengths in the range of 4000–500  $\text{cm}^{-1}$ .

Figure 4 shows the X-ray spectra of the product obtained after the acid treatment of the biomasses. The extracted cellulose from SBH (Figure 4a) and SCB (Figure 4b) displayed a typical cellulose XRD pattern, with a predominance of Cellulose type I. Cellulose I is the most abundant form of cellulose obtained from plants, bacteria, fungi, and algae. Typically, this cellulose consists of two phases, a one-chain triclinic structure corresponding to cellulose  $I_{\alpha}$  and a cellulose  $I_{\beta}$  with a two-chain monoclinic structure [4,5,39].

Diffraction peaks observed in both samples of nanocellulose at  $2\theta$  around  $22^{\circ}$  (plane 200) and  $34^{\circ}$  (plane 004) represent the lattice planes of this cellulose structure that is characteristic of native cellulose [36]. The peak observed around  $12^{\circ}$  (plane 101) in both diffractograms could be attributed to cellulose type II. Additionally, in Figure 4a, a characteristic peak of cellulose II at  $20^{\circ}$  (plane 101) is observed. According to Tao et al. [15], the chemical treatment conditions affect the hydrogen bond and van der Waals force which significantly influences the cellulose's crystallinity and crystal lattice. Sulfuric acid could solubilize the cellulose type I, which is re-precipitated as cellulose type II, and this effect is more pronounced with a long hydrolysis time [11]. In Figure 4b, the diffracted peak observed around  $16^{\circ}$  is presented in lignocellulosic materials [37]. This result suggests that the SCB has a higher resistance to the alkaline treatment than the soybean hulls.

The crystallinity index was calculated from Equation (1), obtaining values between 60 and 63%. This indicates that acid hydrolysis was efficient for obtaining cellulose crystals from SBHs and SCB. The degree of crystallinity of the cellulose obtained was similar to those reported in the literature for microcrystals of various lignocellulosic biomasses, confirming that the method used is feasible, mainly because of its ease and low cost [15,40–43].

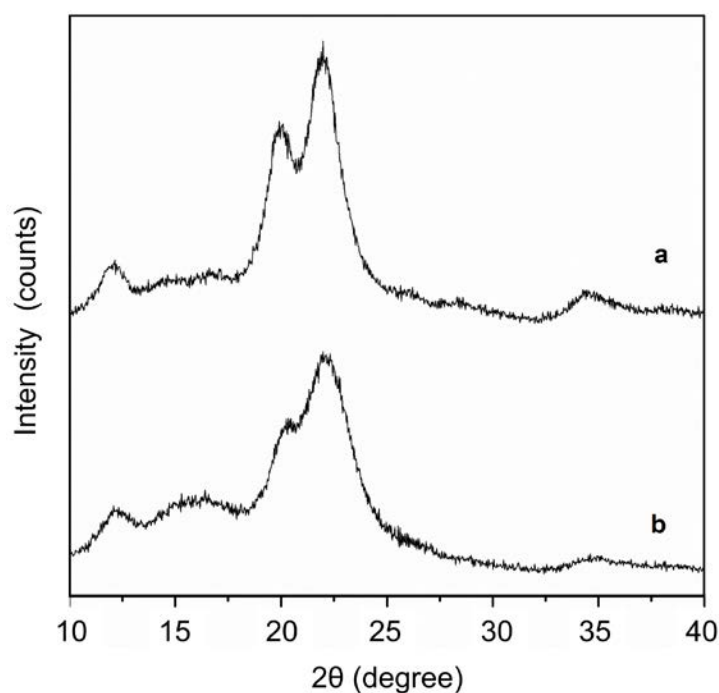


**Figure 4.** X-ray spectrum of cellulose extracted by acid hydrolysis from soybean hulls (a) and sugarcane bagasse (b).

The thermograms of nanocrystalline cellulose from SBHs and SCB are presented in Figure 5. Water loss was observed at around 100 °C, represented by the slightly negative slope at the beginning of the curve for all samples analyzed. For the nanocrystalline cellulose samples (Figure 5a,b), a more pronounced mass reduction was observed between 200 °C and 350 °C when compared to the thermogravimetric curve of the raw samples. It is possible to observe a difference in the decomposition temperature of the starting biomass and nanocellulose, which correlates with the rapid reduction in the molecular weight of cellulose in the biomass during acid hydrolysis.

Moreover, the difference in decomposition between both materials (nanocellulose and raw biomass) observed in Figure 5 is due to the sulfated amorphous regions generated between the cellulose crystals during acid hydrolysis, which make the molecules more accessible to thermal decomposition [8,27,44]. It should be emphasized that the nanocellulose suspension contains cellulose microcrystals and could contain remanent amorphous fractions within the structure. Following the formation of sulfate groups on the nanocellulose surface extracted from cotton (by hydrolysis with H<sub>2</sub>SO<sub>4</sub>), Lin and Dufresne [45] observed initial thermal decomposition at about 150 °C, achieving approximately 30% of weight loss between 150 °C and 250 °C. In this work, the nanocellulose of SBH and SCB showed mass reduction that started at 250 °C, and the peak rate of degradation is reached at approximately 350 °C (Figure 5), suggesting higher thermal resistance compared to the nanocellulose from cotton. It is known that the thermal stability of these nanocrystals is a critical factor in their use as effective reinforcing materials [11,16]. The residue obtained from the SBH is approximately 0.1% at 800 °C, while from SCB it is approximately 10 wt%. The higher residue in the SCB sample could be attributed to the cellulose source and a larger number of sulfate groups formed on the cellulose surface that act as flame retardants [16,46]. Mandal and Chakrabarty [8] reported a similar pattern to nanocellulose in sugarcane bagasse obtained by acid hydrolysis with H<sub>2</sub>SO<sub>4</sub> with residue of 7% at 750 °C.

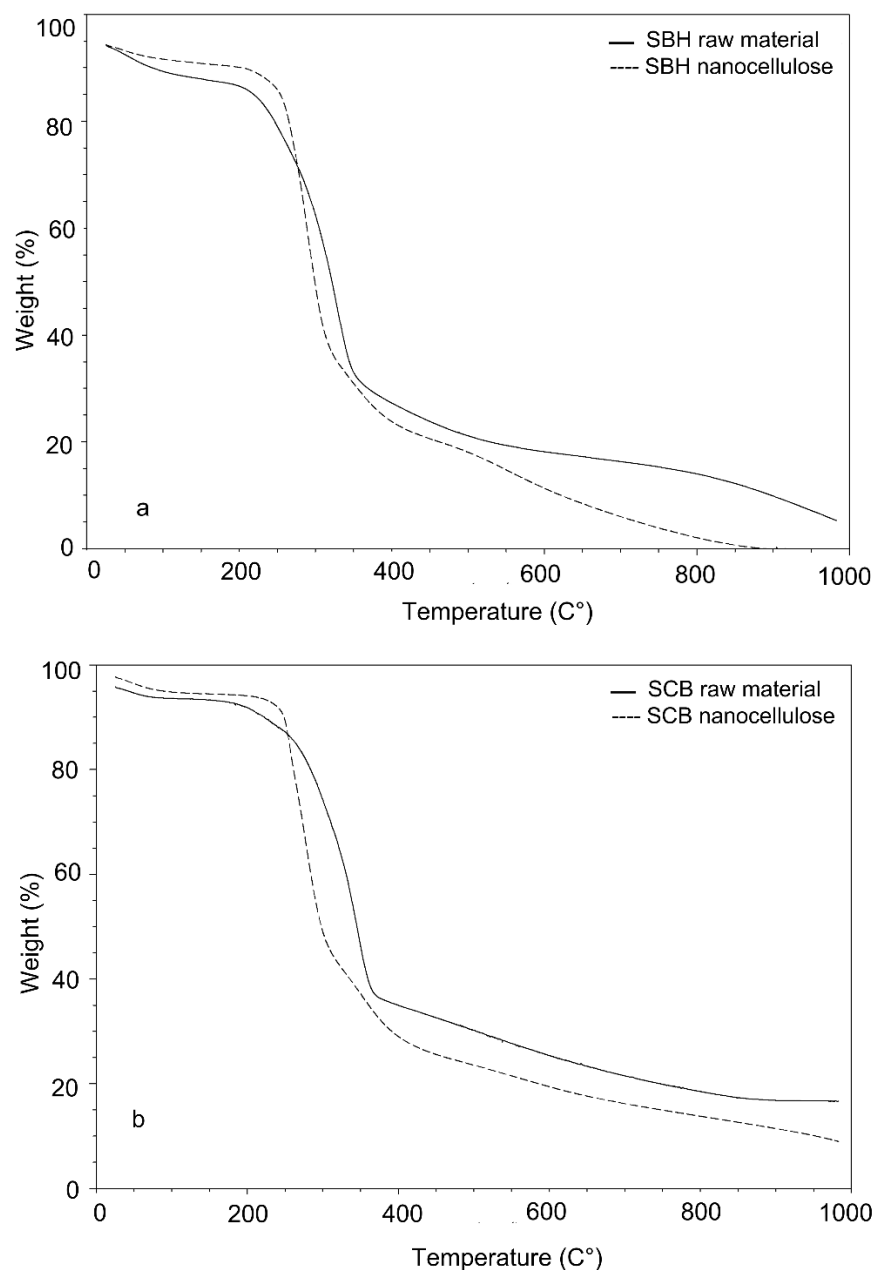


**Figure 5.** TGA thermograms of soybean hull (SBH) nanocellulose and raw soybean hulls (a), sugarcane bagasse (SCB) nanocellulose and raw sugarcane bagasse (b).

The morphology of the biomasses and nanofibers was analyzed by scanning electron microscopy. Figure 6 shows SEM images of nanofibers obtained from soybean hulls and the starting material. Figure 6a shows the surface morphology of the raw soybean hulls, which is characterized by an irregular flat surface, with no fibrous components identified in the structure. In contrast, Figure 6b shows the presence of fibers with a diameter of less than 1  $\mu\text{m}$ . The morphology analysis was made difficult because a freeze-dried sample of the suspension containing nanoparticles was used, resulting in the superposition of layers.

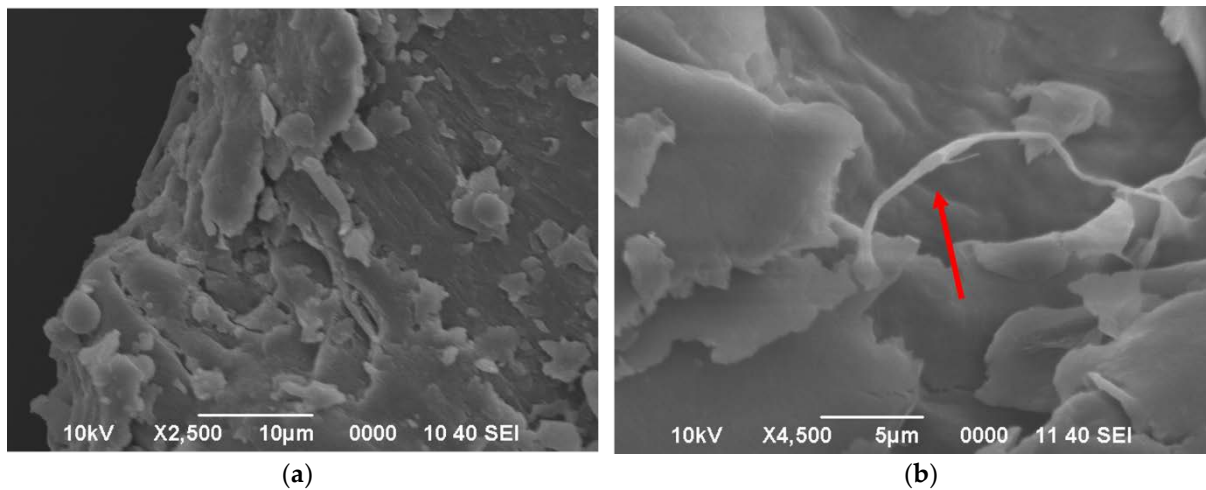


**Figure 6.** Scanning electron microscopy (SEM) of raw soybean hulls (a) and alkali-treated soybean hulls (b).

Numerous reports indicate that acid treatment of previously delignified cellulose removes the amorphous fraction and that nanoscale diameter cellulose fibers are subsequently exposed [8,27,36,44]. Figure 7 shows the AFM images of cellulose nanofibers that were obtained. Figure 7c,d shows a cross-section of the nanocellulose. In both cases, nanoparticles were obtained. The morphology of the SBH was not fibrillar but whisker-like. On the other hand, the SCB nanoparticles exhibited a fibril-like form. The whisker-like form of the SBH nanocellulose obtained was  $230 \pm 42$  nm in diameter and  $12 \pm 2$  nm in height, and the fibril-like form of the SCB nanocellulose was  $103 \pm 30$  nm in diameter and  $6 \pm 3$  nm in height.

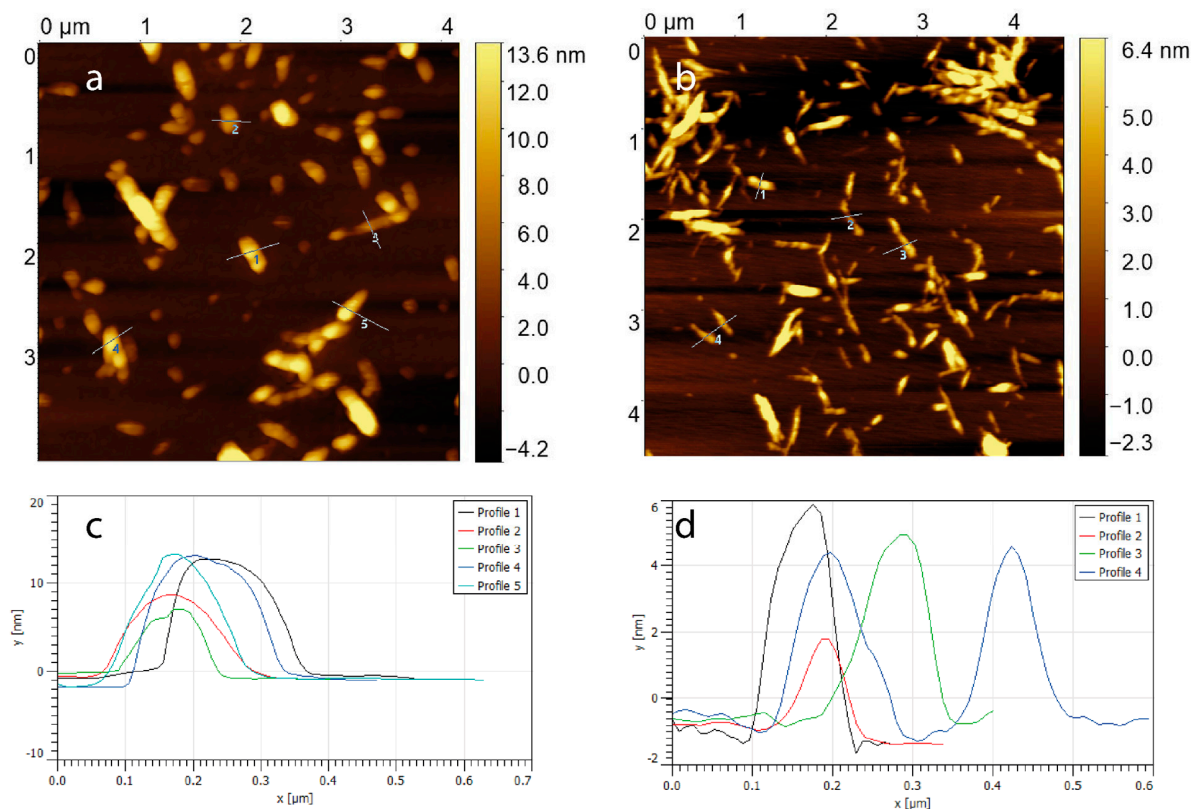


**Figure 7.** AFM images from SBH (a) and SCB (b–d). Cross-section line profiles highlighted in (a,b), respectively.

Camacho et al. [27] observed results close to those observed in this work when they promoted the hydrolysis of pineapple residual peel cellulose with sulfuric acid to obtain nanocrystal. The microscopy's morphological analysis results are similar to other studies where nanocellulose was extracted by acid hydrolysis [11,47,48].

Figure 8 shows the  $\zeta$ -potential of the nanocellulose extracted from the residual biomass. Nanocellulose from SBH and SCB presented a negative zeta-potential at the pH considered (pH 6.83 and 6.58 for SBH and SCB, respectively). The nanocellulose water dispersions from SBH and SCB were stable as the zeta potential was lower than  $-20$  mV [49]. The negatively charged particles are correlated to the surface functionalized with sulfate groups [27,50]. The sulfate ester groups ( $-\text{O}-\text{SO}_3^-$ ) cover the nanocellulose surface, promoting repulsion forces between the particles and favoring its stabilization by dispersion, as proved by AFM [45].

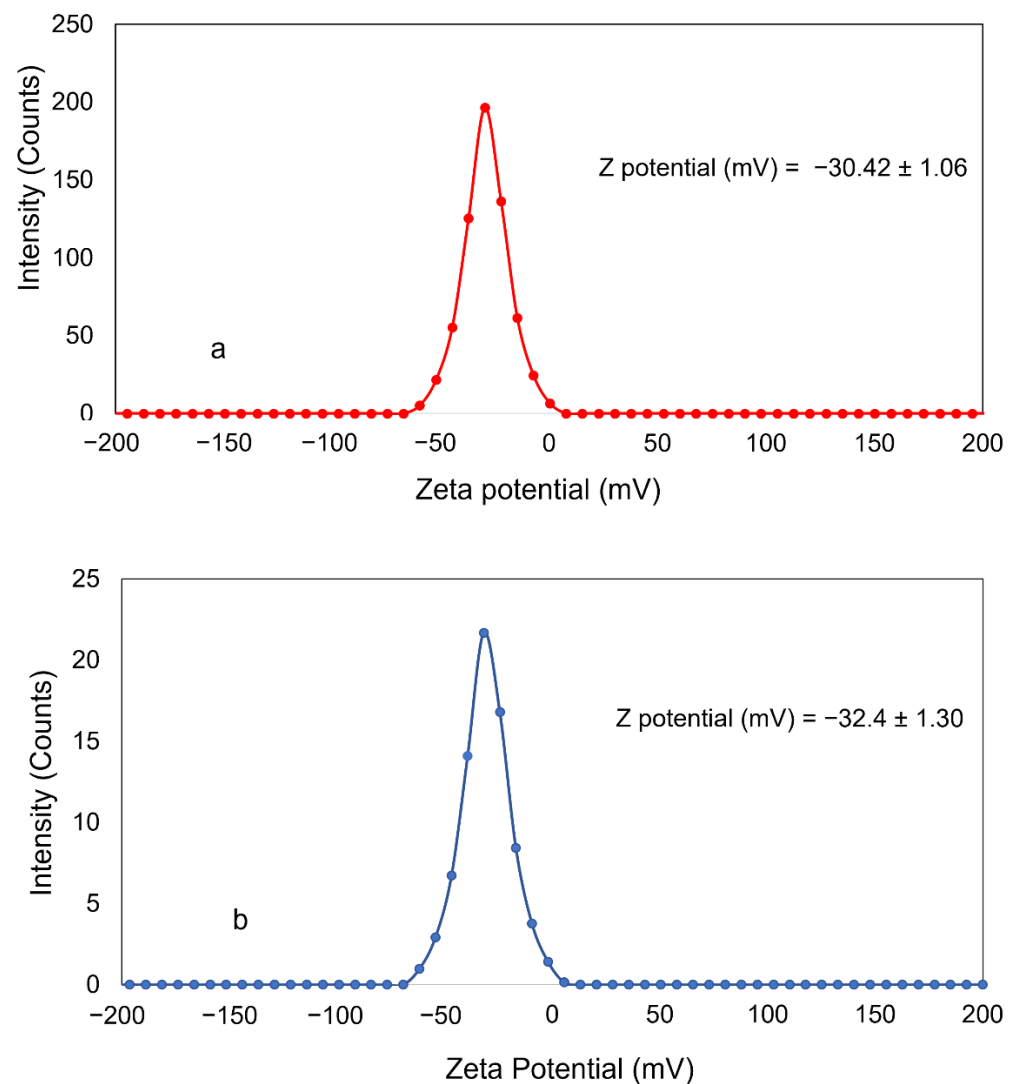


**Figure 8.** Zeta potential of SBH nanocellulose dispersed in water at 0.1 mg/mL concentration and at 6.83 pH (a) and SCB nanocellulose dispersed in water at 0.1 mg/mL concentration and at 6.58 pH (b).

Regarding the DSC thermal analysis, Figure 9 shows the thermograms of the raw soybean hulls and the nanocellulose that was obtained in addition to those of the raw sugarcane bagasse and its respective nanocellulose. All thermograms show endothermic events in the range of temperatures studied. The initial endothermic peak occurred in all cases at temperatures below  $100$  °C due to moisture loss by evaporation. In nanocellulose from sugarcane bagasse, it was observed that the peak was more pronounced than in

the case of the raw samples. This could be associated with the surface of the sulfated cellulose crystals, which may reduce moisture absorption. Mandal and Chakrabarty [8] reported this phenomenon and evaluated nanocrystals obtained from sugarcane bagasse by acid hydrolysis.

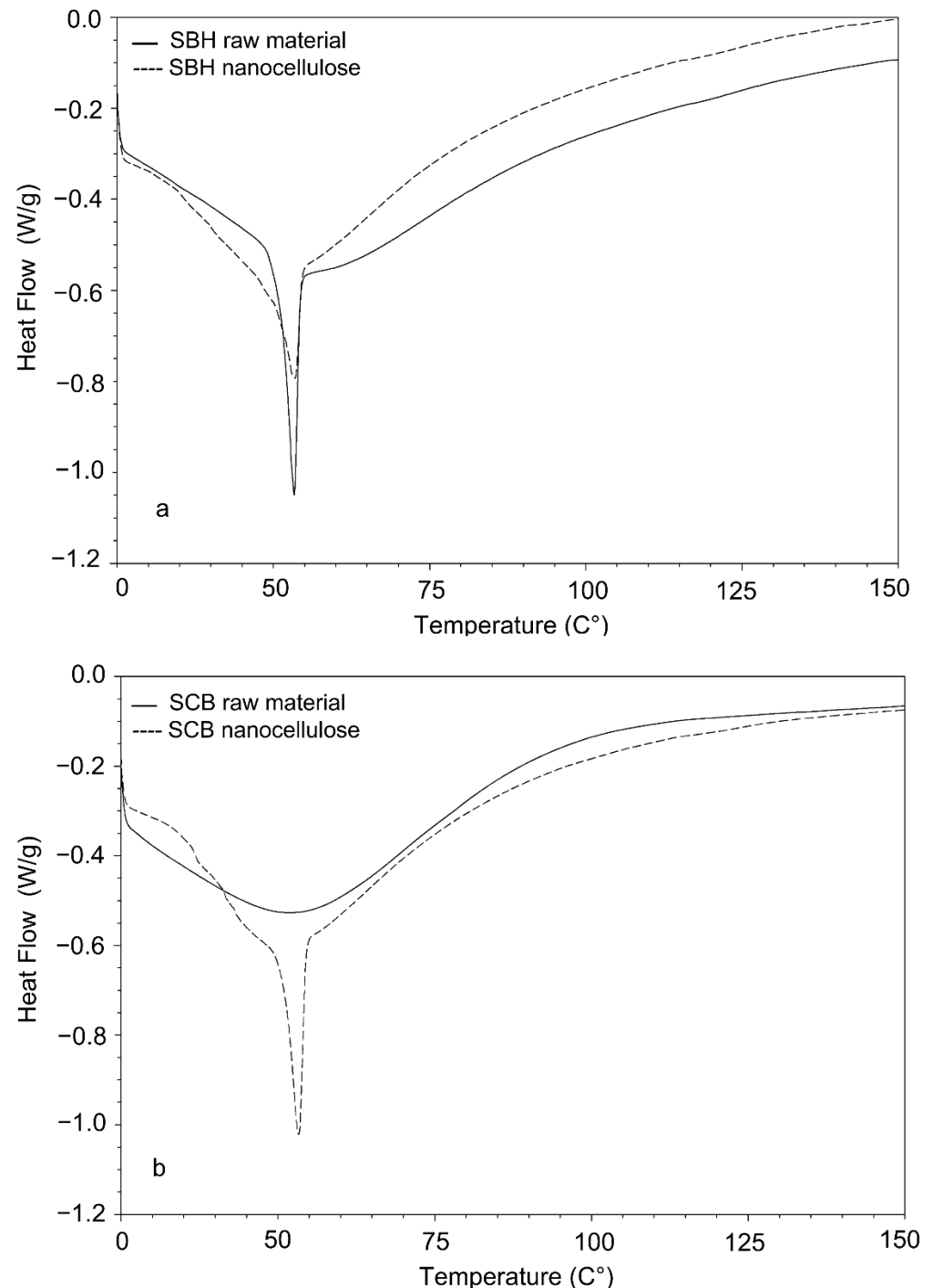


**Figure 9.** DSC curves: (a) raw soybean hulls (SBH) and nanocellulose; (b) raw sugarcane bagasse (SCB) and nanocellulose.

In this work, the acid hydrolysis achieved micro- and nanocellulose yields of 30% and 34% for soybean hull and sugarcane bagasse mass, respectively (data not shown). A similar result (35%) was reported by Pavalaydon et al. [47] using sugarcane bagasse under acid hydrolysis conditions. Using soybean hulls as feedstock in the acid hydrolysis process,

Flauzino Neto et al. [11] achieved nanocellulose yields of 8% and 20% after 30 and 40 min of acid hydrolysis, respectively. Katakajwala et al. [51] reported cellulose and nanocellulose extraction yields of 34% and 15% from soybean hulls and sugarcane bagasse, respectively. In another study, cellulose nanocrystals from royal palm tree agro-industrial waste were obtained by strong acid hydrolysis synthesis at different times and temperatures, achieving yields in the range of 7.8–48.8% [51].

#### 4. Conclusions

In this study, alkaline treatment and consecutive hydrolysis with sulfuric acid and hydrochloric acid was effective for obtaining CNC from soybean hulls and sugarcane bagasse residues, as evidenced by AFM. The products obtained exhibited the forms of fibers and whiskers with a diameter of less than 230 nm and maximum height of 20 nm. A high crystallinity (63%) was determined by XRD analysis; this indicates potential for their application to reinforce other types of materials such as films or polymeric membranes. The nanocellulose from SBH and SCB demonstrated good thermal stability as its degradation temperature started at 250 °C, which indicates its potential for reinforcement of different materials. Furthermore, the nanocrystals were negatively charged and formed stable dispersion in water. Therefore, the present study has significant importance as it indicates an alternative process to produce value-added products, such as CNC, from residual biomass in Paraguay. The data presented can contribute to the implementation of future policies on biomass utilization for production and the installation of biorefinery facilities in Paraguay.

**Author Contributions:** Conceptualization, M.E.V. and O.B.F.; methodology, M.E.V., O.B.F., J.D.R., D.B.M. and Y.C.-U.; formal analysis, M.E.V., O.B.F., J.D.R. and J.R.V.-B.; investigation, M.E.V., O.B.F., J.D.R. and D.B.M.; writing—original draft preparation, J.D.R. and O.B.F.; writing—review and editing, J.D.R., O.B.F., J.R.V.-B. and Y.C.-U. All authors have read and agreed to the published version of the manuscript.

**Funding:** Financial support was received from Consejo Nacional de Ciencia y Tecnología (CONACYT, Paraguay) and the Fondo para la Excelencia de la Educación y la Investigación (FEEI) provided through the project identification PINV18-128.

**Institutional Review Board Statement:** Not applicable for studies not involving humans or animals.

**Informed Consent Statement:** Not applicable.

**Acknowledgments:** The authors would like to thank Hyun Ho Shin for his invaluable assistance.

**Conflicts of Interest:** The authors declare that they have no known competing financial interest or personal relationships that could have appeared to influence the work reported in this paper.

#### Abbreviations

CNC	cellulose nanocrystal
SBHs	soybean hulls
SCB	sugarcane bagasse
ATR-FTIR	attenuated total reflectance Fourier transform infrared spectroscopy
TGA	thermogravimetric analysis
SEM	scanning electron microscopy
AFM	atomic force microscopy
XRD	X-ray diffraction analysis
RPR	residue per product rate
NDF	neutral detergent fiber
ADF	acid detergent fiber
ADL	acid detergent lignin
H	extraction efficiency

$P_1$	mass of micro- and nanocellulose from the acid hydrolysis
$P_0$	mass of feedstock submitted to hydrolysis
$X_0$	cellulose mass fraction in the feedstock
$I_{002}$	maximum intensity at $2\theta = 22.3^\circ$

## References

1. SSEE. Subsecretaría de Estado de Economía 2020. Ministerio de Hacienda. Perfil Económico y Comercial—Paraguay—Junio 2020. Available online: [https://economia.gov.py/application/files/1115/9231/4944/Perfil\\_Economico\\_y\\_Comercial\\_de\\_Paraguay.pdf](https://economia.gov.py/application/files/1115/9231/4944/Perfil_Economico_y_Comercial_de_Paraguay.pdf) (accessed on 20 December 2021).
2. MAG-2022. Ministerio de Agricultura y Ganadería. Síntesis Estadísticas. Available online: <http://www.mag.gov.py/index.php/institucion/dependencias/sintesis-estadistica> (accessed on 20 December 2021).
3. Torgbo, S.; Quan, V.M.; Sukyai, P. Cellulosic value-added products from sugarcane bagasse. *Cellulose* **2021**, *28*, 5219–5240. [CrossRef]
4. Plermjai, K.; Boonyarattanakalin, K.; Mekprasart, W.; Pavasupree, S.; Phoohinkong, W.; Pecharapa, W. Extraction and characterization of nanocellulose from sugarcane bagasse by ball-milling-assisted acid hydrolysis. *AIP Conf. Proc.* **2018**, *2010*, 020005. [CrossRef]
5. Liu, H.M.; Li, H.Y. Application and conversion of soybean hulls. In *Soybean—The Basis of Yield, Biomass and Productivity*; IntechOpen: London, UK, 2017. [CrossRef]
6. Haldar, D.; Purkait, M.K. Micro and nanocrystalline cellulose derivatives of lignocellulosic biomass: A review on synthesis, applications and advancements. *Carbohydr. Polym.* **2020**, *250*, 116937. [CrossRef] [PubMed]
7. Ho, N.W.Y.; Ladisch, M.R.; Sedlak, M.; Mosier, N.; Casey, E. Biofuels from Cellulosic Feedstocks. In *Comprehensive Biotechnology*; Elsevier: Amsterdam, The Netherlands, 2011; pp. 51–62. [CrossRef]
8. Mandal, A.; Chakrabarty, D. Isolation of nanocellulose from waste sugarcane bagasse (SCB) and its characterization. *Carbohydr. Polym.* **2011**, *86*, 1291–1299. [CrossRef]
9. Cowie, J.; Bilek, E.T.; Wegner, T.H.; Shatkin, J.A. Market projections of cellulose nanomaterial-enabled products—Part 2: Volume estimates. *TAPPI J.* **2014**, *13*, 57–69. Available online: <https://www.fs.usda.gov/treearch/pubs/46175> (accessed on 4 April 2022). [CrossRef]
10. Thakur, V.; Guleria, A.; Kumar, S.; Sharma, S.; Singh, K. Recent advances in nanocellulose processing, functionalization and applications: A review. *Mater. Adv.* **2021**, *2*, 1872–1895. [CrossRef]
11. Flauzino Neto, W.P.; Silvério, H.A.; Dantas, N.O.; Pasquini, D. Extraction and characterization of cellulose nanocrystals from agro-industrial residue—Soy hulls. *Ind. Crop. Prod.* **2013**, *42*, 480–488. [CrossRef]
12. Islam, M.T.; Alam, M.M.; Patrucco, A.; Montarsolo, A.; Zoccola, M. Preparation of nanocellulose: A review. *AATCC J. Res.* **2014**, *1*, 17–23. [CrossRef]
13. Kafy, A.; Kim, H.C.; Zhai, L.; Kim, J.W.; Hai, L.V.; Kang, T.J. Cellulose long fibers fabricated from cellulose nanofibers and its strong and tough characteristics. *Sci. Rep.* **2017**, *7*, 17683. [CrossRef]
14. Pang, Z.; Wang, P.; Dong, C. Ultrasonic pretreatment of cellulose in ionic liquid for efficient preparation of cellulose nanocrystals. *Cellulose* **2018**, *25*, 7053–7064. [CrossRef]
15. Tao, P.; Zhang, Y.; Wu, Z.; Liao, X.; Nie, S. Enzymatic pretreatment for cellulose nanofibrils isolation from bagasse pulp: Transition of cellulose crystal structure. *Carbohydr. Polym.* **2019**, *214*, 1–7. [CrossRef] [PubMed]
16. Trache, D.; Tarchoun, A.F.; Derradji, M.; Hamidon, T.S.; Masruchin, N.; Brosse, N.; Hussin, M.H. Nanocellulose: From fundamentals to advanced applications. *Front. Chem.* **2020**, *8*, 392. [CrossRef]
17. Huang, S.; Liu, X.; Chang, C.; Wang, Y. Recent developments and prospective food-related applications of cellulose nanocrystals: A review. *Cellulose* **2020**, *27*, 2991–3011. [CrossRef]
18. Phanthong, P.; Reubroycharoen, P.; Hao, X.; Xu, G.; Abudula, A.; Guan, G. Nanocellulose: Extraction and application. *Carbon Resour. Convers* **2018**, *1*, 32–43. [CrossRef]
19. Rojas, J. Current Trends in the Production of Cellulose Nanoparticles and Nanocomposites for Biomedical Applications. In *Cellulose: Fundamental Aspects and Current Trends*; Bedoya, M., Ed.; IntechOpen: London, UK, 2015; pp. 193–228.
20. Wang, N.; Ding, E.; Cheng, R. Preparation and liquid crystalline properties of spherical cellulose nanocrystals. *Langmuir* **2008**, *24*, 5–8. [CrossRef] [PubMed]
21. Li, D.; Henschen, J.; Ek, M. Esterification and hydrolysis of cellulose using oxalic acid dihydrate in a solvent-free reaction suitable for preparation of surface-functionalised cellulose nanocrystals with high yield. *Green Chem.* **2017**, *19*, 5564–5567. [CrossRef]
22. Bian, H.; Luo, J.; Wang, R.; Zhou, X.; Ni, S.; Shi, R.; Dai, H. Recyclable and reusable maleic acid for efficient production of cellulose nanofibrils with stable performance. *ACS Sustain. Chem. Eng.* **2019**, *7*, 20022–20031. [CrossRef]
23. Yu, H.; Abdalkarim, S.Y.H.; Zhang, H.; Wang, C.; Tam, K.C. Simple process to produce high-yield cellulose nanocrystals using recyclable citric/hydrochloric acids. *ACS Sustain. Chem. Eng.* **2019**, *7*, 4912–4923. [CrossRef]
24. Bian, H.; Dong, M.; Chen, L.; Zhou, X.; Wang, R.; Jiao, L.; Dai, H. On-demand regulation of lignocellulosic nanofibrils based on rapid fractionation using acid hydrotrope: Kinetic study and characterization. *ACS Sustain. Chem. Eng.* **2020**, *8*, 9569–9577. [CrossRef]

25. Cheng, M.; Qin, Z.; Hu, J.; Liu, Q.; Wei, T.; Li, W. Facile and rapid one-step extraction of carboxylated cellulose nanocrystals by H<sub>2</sub>SO<sub>4</sub>/HNO<sub>3</sub> mixed acid hydrolysis. *Carbohydr. Polym.* **2020**, *231*, 115701. [[CrossRef](#)]
26. Jiang, F.; Hsieh, Y.L. Chemically and mechanically isolated nanocellulose and their self-assembled structures. *Carbohydr. Polym.* **2013**, *95*, 32–40. [[CrossRef](#)] [[PubMed](#)]
27. Camacho, M.; Ureña, Y.R.; Lopretti, M.; Carballo, L.B.; Moreno, G.; Alfaro, B.; Baudrit, J.R. Synthesis and characterization of nanocrystalline cellulose derived from pineapple peel residues. *J. Renew. Mater.* **2017**, *5*, 271–279. [[CrossRef](#)]
28. Fotie, G.; Limbo, S.; Piergiovanni, L. Manufacturing of food packaging based on nanocellulose: Current advances and challenges. *Nanomaterials* **2020**, *10*, 1726. [[CrossRef](#)] [[PubMed](#)]
29. Koopmans, A.; Koppejan, J. Agricultural and Forest Residues Generation, Utilization, and Availability. In Proceedings of the Regional on Modern Applications of Biomass Energy, Kuala Lumpur, Malaysia, 6–10 January 1997. Available online: <http://www.fao.org/3/ad576e/ad576e00.pdf> (accessed on 20 May 2022).
30. Rodas, R.I.; Cano, V.E.; Frutos, M.L. Análisis de la cadena de valor de la soja en el Paraguay: Chain value analysis of soybean and its manufactures in Paraguay. *S. Fla. J. Dev.* **2021**, *2*, 7412–7429. [[CrossRef](#)]
31. Fleck, J.C. Estudio de Factibilidad Económica del Uso del Bagazo de Caña de Azúcar para la Obtención de Papel de Impresión y Escritura en el Paraguay. Master's Thesis, Universidad Nacional de Misiones, Garupá, Argentina, 2009.
32. Research and Market. 2022. Available online: <https://www.researchandmarkets.com/reports/5009171/global-nanocellulose-market-by-type-mfc-and-nfc#rela4-5305030> (accessed on 20 May 2022).
33. Dorrestijn, E.; Laarhoven, L.J.J.; Arends, I.W.C.E.; Mulder, P. The occurrence and reactivity of phenoxyl linkages in lignin and low rank coal. *J. Anal. Appl. Pyrolysis* **2000**, *54*, 153–192. [[CrossRef](#)]
34. Merci, A.; Urbano, A.; Grossmann, M.V.E.; Tischer, C.A.; Mali, S. Properties of microcrystalline cellulose extracted from soybean hulls by reactive extrusion. *Food Res. Int.* **2015**, *73*, 38–43. [[CrossRef](#)]
35. Huang, S.; Zhou, L.; Li, M.C.; Wu, Q.; Zhou, D. Cellulose nanocrystals (CNCs) from corn stalk: Activation energy analysis. *Materials* **2017**, *10*, 80. [[CrossRef](#)]
36. Nang An, V.; Nhan, C.; Thuc, H.; Tap, T.D.; Van, T.T.T.; Van Viet, P.; Van Hieu, L. Extraction of high crystalline nanocellulose from biorenewable sources of Vietnamese agricultural wastes. *J. Polym. Environ.* **2020**, *28*, 1465–1474. [[CrossRef](#)]
37. Debiagi, F.; Faria-Tischer, P.; Mali, S. Nanofibrillated cellulose obtained from soybean hull using simple and eco-friendly processes based on reactive extrusion. *Cellulose* **2020**, *27*, 1975–1988. [[CrossRef](#)]
38. Pappas, C.; Tarantilis, P.A.; Daliani, I.; Mavromoustakos, T.; Polissiou, M. Comparison of classical and ultrasound-assisted isolation procedures of cellulose from kenaf (*Hibiscus cannabinus* L.) and eucalyptus (*Eucalyptus rodustrus* Sm.). *Ultrason. Sonochemistry* **2002**, *9*, 19–23. [[CrossRef](#)]
39. Sugiyama, J.; Vuong, R.; Chanzy, H. Electron diffraction study on the two crystalline phases occurring in native cellulose from an algal cell wall. *Macromolecules* **1991**, *24*, 4168–4175. [[CrossRef](#)]
40. Frone, A.N.; Chiulan, I.; Panaitescu, D.M.; Nicolae, C.A.; Ghiurea, M.; Galan, A.M. Isolation of cellulose nanocrystals from plum seed shells, structural and morphological characterization. *Mater. Lett.* **2017**, *194*, 160–163. [[CrossRef](#)]
41. Coelho, C.C.; Michelin, M.; Cerqueira, M.A.; Gonçalves, C.; Tonon, R.V.; Pastrana, L.M.; Freitas-Silva, O.; Vicente, A.A.; Cabral, L.M.; Teixeira, J.A. Cellulose nanocrystals from grape pomace: Production, properties and cytotoxicity assessment. *Carbohydr. Polym.* **2018**, *192*, 327–336. [[CrossRef](#)] [[PubMed](#)]
42. Sainorudin, M.H.; Abdullah, N.A.; Rani, M.S.; Mohammad, M.; Abd Kadir, N.H.; Razali, H.; Asim, N.; Yaakob, Z. Investigation of the structural, thermal and orphological properties of nanocellulose synthesised from pineapple leaves and sugarcane bagasse. *Curr. Nanosci.* **2022**, *18*, 68–77. [[CrossRef](#)]
43. Hernandez, J.A.; Soni, B.; Iglesias, M.C.; Vega-Eramuspe, I.B.; Frazier, C.E.; Peresin, M.S. Soybean hull pectin and nanocellulose: Tack properties in aqueous pMDI dispersions. *J. Mater. Sci.* **2022**, *57*, 5022–5035. [[CrossRef](#)]
44. Kim, D.Y.; Lee, B.M.; Koo, D.H.; Kang, P.H.; Jeun, J.P. Preparation of nanocellulose from a kenaf core using E-beam irradiation and acid hydrolysis. *Cellulose* **2016**, *23*, 3039–3049. [[CrossRef](#)]
45. Lin, N.; Dufresne, A. Surface chemistry, morphological analysis and properties of cellulose nanocrystals with gradiented sulfation degrees. *Nanoscale* **2014**, *6*, 5384–5393. [[CrossRef](#)]
46. Roman, M.; Winter, W.T. Effect of sulfate groups from sulfuric acid hydrolysis on the thermal degradation behavior of bacterial cellulose. *Biomacromolecules* **2004**, *5*, 1671–1677. [[CrossRef](#)]
47. Pavalaydon, K.; Ramasawmy, H.; Surroop, D. Comparative evaluation of cellulose nanocrystals from bagasse and coir agro-wastes for reinforcing PVA-based composites. *Environ. Dev. Sustain.* **2022**, *24*, 9963–9984. [[CrossRef](#)]
48. Gond, R.K.; Gupta, M.K.; Jawaid, M. Extraction of nanocellulose from sugarcane bagasse and its characterization for potential applications. *Polym. Compos.* **2021**, *42*, 5400–5412. [[CrossRef](#)]
49. Andrade, F.K.; Morais, J.P.S.; Muniz, C.R.; Nascimento, J.H.O.; Vieira, R.S.; Gama, F.M.P.; Rosa, M.F. Stable microfluidized bacterial cellulose suspension. *Cellulose* **2019**, *26*, 5851–5864. [[CrossRef](#)]
50. Lee, H.V.; Hamid, S.B.A.; Zain, S.K. Conversion of lignocellulosic biomass to nanocellulose: Structure and chemical process. *Sci. World J.* **2014**, *2014*, 631013. [[CrossRef](#)] [[PubMed](#)]
51. Katakajwala, R.; Mohan, S.V. Multi-product biorefinery with sugarcane bagasse: Process development for nanocellulose, lignin and biohydrogen production and lifecycle analysis. *Chem. Eng. J.* **2022**, *446*, 137233. [[CrossRef](#)]